Macromolecules

pubs.acs.org/Macromolecules Article

Diblock Copolymer Blends Do Not Mimic Metal Alloys

Zachary M. Gdowski, Samuel M. Swartzendruber, Mahesh K. Mahanthappa,* and Frank S. Bates*

Cite This: *Macromolecules* 2024, 57, 7926–7940 Read Online

ACCESS | Metrics & More | Article Recommendations | Supporting Information

ABSTRACT: Periodic particle packings are ubiquitous across many forms of condensed matter including colloids, metals, and block polymers. We report the morphologies of binary blends of compositionally asymmetric poly(ethylene-*alt*-propylene)-*block*-poly(ethylene oxide) (PEP-PEO) and PEP-*block*-poly(dimethylsiloxane) (PEP-PDMS) diblock copolymers based on small-angle X-ray scattering measurements. Strong thermodynamic incompatibility of the minority blocks results in discrete particles containing PEO and PDMS cores with common PEP coronae in the mixtures. Nearly identical particle radii, i.e., within ∼10% including the core and corona segments, lead to rapid formation of solid solutions with BCC symmetry at all compositions when the disordered mixtures are cooled below the order-to-disorder transition temperature. Increasing the pure component particle radius ratio to $R_{PEP\text{-}PEO}/R_{PEP\text{-}PDMS} \approx 1.2$ greatly retards nucleation and growth of order, restricting the development of BCC packing, with limited formation of the Laves C14 phase anticipated by self-consistent mean-field theory. Surprisingly, the added degrees of freedom in the two-component system, naively expected to favor complex tetrahedral packings, detract from the well-established behavior of single component, sphere-forming diblock copolymers, where interparticle chain exchange leads to various Frank–Kasper phases. This striking and unanticipated behavior is attributed to frustrated dynamics associated with the combined effects of restricted chain exchange and jammed space-filling soft particles.

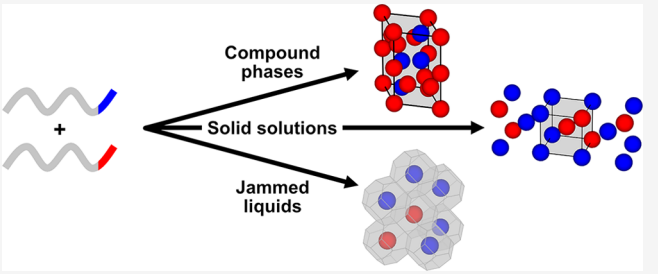

INTRODUCTION

Recent self-consistent mean-field theory (SCFT) calculations describe the phase behavior of mixtures of compositionally asymmetric AB and A′C diblock copolymers ($f_B = f_C = 0.2$), where the minority B and C blocks are thermodynamically incompatible, i.e. $\chi_{AB} \cong \chi_{AC} < \chi_{BC}$, in which χ is the effective interaction parameter.[1,2] The associated phase diagram, determined with $N_{AB}/N_{A'C} = 1.3$ where N is the degree of polymerization, closely resembles certain binary metal alloy phase diagrams that are characterized by a eutectic invariant and several 2-phase regions.[3] A particularly noteworthy feature is a narrow Laves C14 compound phase field ($MgZn_2$ intermetallic structure type) separating two expansive C14/BCC 2-phase windows at moderate values of $(\chi\langle N\rangle)_{AB} \cong (\chi\langle N\rangle)_{AC} > 25$, where $(\chi\langle N\rangle)_{ODT} \cong 22$; $\langle N\rangle$ is the average degree of polymerization. This equilibrium phase diagram illustrates striking analogies between micelle forming diblock copolymer blends and metal alloys. A critical factor associated with Laves phase formation in metal alloys is a specific ratio of atomic radii exemplified by $MgZn_2$ ($R_{Mg}/R_{Zn} = 1.20$) and $MgCu_2$ ($R_{Mg}/R_{Cu} = 1.25$), which form C14 and related C15 compounds, respectively.[4−8]

Motivated by these predictions, we devised a model system of particle-forming diblock copolymers, nominally mimicking metal alloys, to evaluate the feasibility of producing Laves phases, while avoiding more complex molecular architectures, such as $B_1AB_2CB_3$ multiblock terpolymers, predicted to form a host of particle-based morphologies.[9] Surprisingly little has been published on mixing AB and A′C diblock copolymers. Frielinghaus et al. investigated the phase behavior of binary blends of polystyrene-*block*-polyisoprene (PS-PI) and polyisoprene-*block*-poly[ethylene oxide (EO)] (PI-PEO) blends.[10,11] While the PI block volume fractions $f_{PI} \approx 0.5$, 0.6, or 0.7 produced hexagonally packed cylinders (HEX) or lamellae as pure components, the mixtures macroscopically phase separated at most compositions due to large differences in the domain spacings of the components. Ishizu et al. prepared sets of PS-PI and PS-P2VP (P2VP = poly(2-vinylpyridine)) including one pair that formed spherical domains of PI and P2VP in a PS matrix. However, a 5-fold difference in polymer molecular weights resulted in a random arrangement of small and large particles.[12] Finally, Abbas and Lodge reported the emergence of the AB_{13}-type superlattice ($NaZn_{13}$ analog)[13] in blends of PS-PI and PS-PDMS in the PS-selective solvent diethyl phthalate, drawing analogies with hard colloidal systems containing spherical particles with significantly different radii.[14,15] However, the presence of a corona-

Received: May 20, 2024
Revised: July 18, 2024
Accepted: July 23, 2024
Published: August 14, 2024

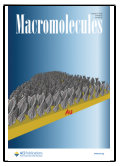

https://doi.org/10.1021/acs.macromol.4c01146
Macromolecules 2024, 57, 7926−7940

selective solvent limits direct comparison to the undiluted melt theory.

In the present work, we synthesized PEP-PEO and PEP-PDMS diblocks with asymmetric compositions to produce particles with spherical poly(EO) (PEO) and poly(dimethylsiloxane) (PDMS) cores and common poly(ethylene-*alt*-propylene) (PEP) corona blocks. The relative thermodynamic incompatibility between PEO and PDMS versus each core and corona block, based on the interaction parameters $\chi_{PEP\text{-}PDMS} < \chi_{PEP\text{-}PEO} < \chi_{PEO\text{-}PDMS}$, and the choice of suitable molecular weights ensures that the core blocks produce discrete micelles, i.e., the chemically distinct core blocks do not mix in the ordered states, or when disordered near the order-to-disorder transition temperature (T_{ODT}). Two conditions were explored in binary mixtures of these compounds: $\alpha = R_{PEP\text{-}PEO}/R_{PEP\text{-}PDMS} \approx 0.9$ and 1.2, where R refers to the average total particle radius including the core and corona of the nominally spherical micelles. Blends were formed by solvent casting and their self-assembled structures were determined by small-angle X-ray scattering (SAXS) as a function of composition, temperature, and thermal history. The results demonstrate surprising nonideality for the $\alpha \approx 1.2$ blends, including retarded nucleation and growth of order when the disordered liquid is cooled below T_{ODT}, and limited formation of the C14 Laves phase. Conversely, with $\alpha \approx 0.9$ the mixtures rapidly form solid solution BCC crystals when cooled from disorder at all compositions. These findings are discussed in the context of restricted chain exchange combined with steric barriers to rearranging the local packing of dissimilarly sized particles, which together result in highly frustrated ordering dynamics.

EXPERIMENTAL METHODS

Materials. All reagents were purchased from Sigma-Aldrich Chemical Co. and used as received, unless otherwise noted. Isoprene (99%) and EO (99.5%) were both distilled under vacuum after stirring for 1 h over *n*-butyl lithium or butylmagnesium chloride, respectively, at 0 °C. Hexamethylcyclotrisiloxane (D_3) (98%, Acros Organics) was purified either by successive sublimation and stirring over dibutyl magnesium for 2 h at 80 °C (for PD1) or successive stirring over calcium hydride for 4 h at 90 °C and over dibutyl magnesium for 1 h at 90 °C (for PD2 and PD3). Anhydrous cyclohexane (Fisher Scientific International, Inc.) was purified by passage through activated alumina and Q5 catalyst, and tetrahydrofuran through activated alumina using a custom-built system. Hexamethylphosphoramide (HMPA) and trimethylsilyl chloride (TMSCl) were stirred for >24 h over CaH_2, distilled, and stored under argon or nitrogen.

Synthesis of Diblock Polymers. Diblock copolymers were synthesized by anionic polymerization under an air- and water-free argon atmosphere using previously established procedures.[16,17] In brief, isoprene polymerization was initiated with 1.4 M *sec*-butyl lithium in dry cyclohexane, and reacted for 4 h at 40 °C. Either EO for PEP-PEO or D_3 in dry cyclohexane for PEP-PDMS was added and allowed to react overnight to end-cap the 1,4-polyisoprene block. For PDMS blocks, HMPA was then added at 0 °C and reacted for 25 min, followed by termination with TMSCl at about 90% conversion to minimize side reactions.[16] After termination, sodium bicarbonate solution in distilled water was added to the reactor, and the cyclohexane solution was washed with distilled H_2O until neutralized. For PEP-PEO diblocks, the EO-end-capped 1,4-polyisoprene was treated with isopropanol and the PI-OH was hydrogenated to yield PEP-OH (vide infra), followed by azeotropic freeze-drying from benzene. A THF solution of this PEP-OH was then titrated with potassium naphthalenide until a faint, olive-green color persisted, after which EO was added. After reacting for 2 d at 40 °C, this polymerization was terminated using a degassed mixture of 100:1 *v*/*v* CH_3OH: conc. HCl(*aq*). EO polymerizations were run to ∼50−60% conversion. The resulting solution was vacuum-filtered and THF was removed using rotary evaporation. The resulting polymer was then redissolved in CH_2Cl_2 and extracted with ∼1 vol % NaCl(*aq*) in distilled H_2O. After separation, CH_2Cl_2 was removed by rotary evaporation, and the polymer was dissolved in benzene and azeotropically freeze-dried.

Hydrogenation of Block Polymers. Both PEP-PDMS and PEP-OH were prepared by catalytic hydrogenation of polyisoprene. PI-PDMS diblocks were saturated using a modified version of a previously published procedure.[18] Pd/$CaCO_3$ (5 wt %, unpoisoned, Strem Chemicals) was added to a 0.3 L Parr 452HC reactor, which was subsequently evacuated for 1 h at room temperature and then overnight at 100 °C. The reactor then was charged with 100 psi H_2(*g*) (Airgas) and heated to 100 °C for 1 h to activate the catalyst, after which it was cooled and vented at 25 °C and filled with ∼5 psig Ar(*g*). A degassed solution of PI-PDMS in cyclohexane (0.01 g/mL), prepared in a custom sealable Erlenmeyer flask that was sparged with argon for 1 h, was added to the reactor under argon pressure to maintain an air-free environment. Hydrogenation reactions were performed for at least 24 h at 70 °C and 500−600 psi H_2 to effect >98% catalytic saturation. For PEP-PEO syntheses, PI-OH was dissolved in cyclohexane and added to a 1 L Parr 236HC reactor with a PtRe/SiO_2 catalyst (Dow Chemical Co.) in a [polymer/catalyst] = 20:1 mass ratio. The reactor was sparged with Ar(*g*) for 30 min, and the reactions were conducted under 500−600 psi H_2 at 70 °C for 12 h to achieve >99% olefin saturation. Polymers were isolated from the catalysts by high-pressure Ar(*g*) filtration through a 0.22 μm Durapore Membrane Filter and they were precipitated in chilled CH_3OH.

Nuclear Magnetic Resonance (NMR) Spectroscopy. Quantitative ^{1}H Nuclear Magnetic Resonance (NMR) spectra were obtained on a Bruker Avance III HD 400 MHz spectrometer in $CDCl_3$ using a 10 s pulse repetition delay, from which molecular weights were calculated by end group analyses.

Size Exclusion Chromatography (SEC). Size Exclusion Chromatography (SEC) analyses of for PI-PDMS and PEP-PDMS employed three Agilent PLgel Mixed-C columns and a Waters 2410 RI Detector using THF inhibited with BHT as the eluent. The instrument was calibrated using 10 narrow dispersity polystyrene standards (M_p = 580−377400 g/mol supplied by Agilent Technologies). SEC measurements were conducted for PI-OH, PEP-OH, and PEP-PEO using a similarly calibrated Viscotek GPCMax VE 2001 system with two Agilent PLgel Mixed-B columns and a Viscotek VE 3580 RI Detector with uninhibited THF as the eluent. All samples were prepared with concentrations ∼3−5 mg/mL THF and filtered through a 0.22 μm syringe filter prior to measurement.

Blending. A weighted average of homopolymer densities at 140 °C (see footnote in Table 1) was used to convert from a desired volume fraction to a mass fraction of each diblock copolymer. All pure component and blend specimens were prepared for SAXS analyses by

Table 1. Diblock Copolymer Molecular Characteristics

polymer	M_n (kg/mol)[a]	f_{core}[b]	N_v[b]	$Đ$[c]
PD1	13.5	0.161	249	1.07
PD2	13.5	0.144	237	1.06
PD3	15.7	0.184	272	1.07
PO1	10.8	0.055	203	1.09
PO2	15.4	0.068	268	1.07

[a]Number-average molecular weight measured by ^{1}H NMR spectroscopy. [b]Core volume fraction and volume-referenced degree of polymerization calculated from ^{1}H NMR using homopolymer block densities at 413 K (ρ_O = 1.06 g/cm^3, ρ_D = 0.895 g/cm^3, ρ_P = 0.790 g/cm^3) relative to a v = 118 Å^3 reference volume.[28] [c]Dispersity determined by SEC with polystyrene standard calibration.

https://doi.org/10.1021/acs.macromol.4c01146
Macromolecules 2024, 57, 7926−7940

solvent casting from THF, which is a good solvent for all three blocks, albeit somewhat preferential for PEO over PDMS based on homopolymer solubility parameters.[19,20] All PEP-PEO diblocks were freeze-dried (again) prior to use to remove residual water. Blends were prepared in a 50 mg/mL THF solution and cast onto microscope slides by passing a stream of $N_2(g)$ over the slide for 10−15 min. The resulting films were then dried under vacuum (∼50 mTorr), loaded in differential scanning calorimetry (DSC) pans (DSC Consumables, Inc.), and sealed under Ar(g). Blends were annealed at 50 °C for 24 h prior to analysis, unless noted.

Small-Angle X-ray Scattering (SAXS). Synchrotron SAXS measurements were conducted at the Sector 12-ID-B or Sector 5-ID-D beamlines of the Advanced Photon Source at Argonne National Laboratory (Lemont, IL) or Sector 11-BM beamline at the National Synchrotron Light Source II at Brookhaven National Laboratory (Upton, NY). At Sector 12-ID-B, experiments used an incident X-ray wavelength λ = 0.932 Å, a sample-to-detector distance (SDD) of 2.00 or 3.61 m, an exposure time of 0.1 s, and a beam size of 100 μm × 140 μm; simultaneous SAXS/wide-angle X-ray scattering (WAXS) data were collected using both Pilatus 2 M and Pilatus 300 K detectors. At Sector 5-ID-D, experiments were performed with λ = 0.729 Å, a SDD of 8.50 m, an exposure time of 1.0 s, a beam size of 250 μm × 250 μm and a Rayonix MX170HS detector. At Sector 11-BM, experiments used λ = 0.918 Å, a 5.02 m SDD, an exposure time of 3.0 s, a beam size of 200 μm × 200 μm, and a Pilatus 2 M detector. Instrument calibrations at Sectors 12-ID-B and 11-BM were accomplished with silver behenate (d = 58.39 Å) and at Sector 5-ID-D using Au-coated Si with 7200 lines/mm.

Lab-source SAXS measurements employed a Xenocs Ganesha instrument equipped with a GeniX 3D Cu microfocus X-ray tube source (λ = 1.54 Å) with a fully evacuated flight path, a 1.05 m SDD, and an exposure time of 5 min on a Dectris Eiger R 1 M detector. Samples were loaded into aluminum sandwich cells fitted with a Viton O-ring and two Kapton windows to prevent flow out of the beam path upon disordering. All 2D-SAXS patterns were azimuthally integrated using software available at each beamline or the Datasqueeze free software package[21] to obtain 1D scattering intensity profiles $I(q)$ vs q (Å^{-1}), where $q = (4\pi/\lambda)\sin(\theta/2)$ is the scattering wavevector and θ is the scattering angle. 1D traces were indexed using a freely available Igor Pro (Wavemetrics, Inc.) macro.[22] All presented SAXS data were acquired after 10 °C/min temperature changes followed by quiescent annealing for 10 min prior to measurement unless noted.

Form Factor Fitting. SAXS traces were manually background subtracted in IgorPro by removing the Bragg scattering peaks from the data and fit with polydispersity-modified spherical form factors in SasView version 5.0.6. Contrast factors were estimated based on the polymer melt densities given in Table 1.

Dynamic Mechanical Spectroscopy (DMS). Linear viscoelastic data were obtained on a TA Instruments Rheometric Series ARES-1 instrument using an 8 mm parallel plate geometry with ∼0.5 mm gap size. Dynamic elastic storage (G') and loss (G'') shear moduli were measured at fixed temperatures over the frequency range $0.1 \le \omega \le 100$ rad/s, or while heating and cooling ($dT/dt \le 5$ °C/min) with ω = 1 rad/s.

Differential Scanning Calorimetry. DSC data were obtained using a TA Instruments Q1000 instrument. All samples were loaded into hermetically sealed aluminum TZero DSC pans (supplied by DSC Consumables, Inc. or TA Instruments, Inc.) and measured using a 10 °C/min temperature ramp rate. Crystallization temperatures are reported on first cooling and melting temperatures are reported on second heating.

RESULTS AND ANALYSIS

The goal of this study was to uncover the mixing behavior of pairs of particle-forming diblock copolymers that share a common majority (corona) block and have thermodynamically incompatible minority (core) blocks. The choice of PEP-PEO (also referred to as PO) and PEP-PDMS (also referred to as PD) satisfies these criteria, based on the associated effective segment interaction parameters: $\chi_{OD} > \chi_{PO} > \chi_{PD}$ as estimated from the solubility parameters δ_O = 9.9, δ_P = 7.9 and δ_D = 7.4 (cal/cm^3)$^{1/2}$.[19,20] Hence, the core blocks are expected to be immiscible and form separate microdomains on blending the PO and PD diblocks. However, this combination of diblocks introduces significant molecular constraints. Based on analogies with metal alloys, we anticipated the need to generate relatively similar particle dimensions, while maintaining proximity to T_{ODT} to facilitate melt processing and to minimize nonequilibrium effects. We approached this design challenge by first identifying the molecular parameters associated with obtaining nominally spherical particles with the PD system over an experimentally tractable range of temperatures, followed by considerations in synthesizing suitable PO specimens.

Identifying the appropriate composition and molecular weight of each diblock component in the targeted blends is complicated by conformational asymmetry, which skews the predicted AB diblock copolymer phase portrait.[20,23−27] With different statistical segment lengths, $b_A > b_B$, the range of A-rich particle-forming compositions is expanded for $f_A \to 0$ and reduced for $f_A \to 1$, where $b = R_g/(N_v/6)^{1/2}$ in which R_g is the radius of gyration and N_v is the degree of polymerization referenced to a common segment volume v. PO and PD are both conformationally asymmetric, based on the statistical segment lengths b_P = 0.76 nm, b_O = 0.79 nm, and b_D = 0.54 nm referenced to v = 118 Å^3.[19] Therefore, PD diblock polymers that produce particles with PDMS cores are characterized by a restricted range of compositions and temperatures relative to PO diblocks comprising PEO cores. For this reason, we first focused on the PD phase behavior, followed by preparation of PO specimens. Narrow dispersity, compositionally asymmetric diblock polymers with majority PEP blocks and minority PDMS and PEO blocks were synthesized and characterized as summarized in Table 1; NMR and SEC data are given in Figures S1−S10.

Design of PD Diblock Copolymer. In order to identify suitable molecular parameters for the preparation of a particle forming PD specimen for blending with PO polymers, we synthesized PD2 and PD3 with the compositions and molecular weights listed in Table 1. A SAXS pattern obtained at room temperature (Figure S11A) demonstrates that PD2 produces a single low-intensity and broad scattering peak indicative of a disordered state (DIS). PD3 is characterized by sharp Bragg peaks that persist up to 100 °C at $q/q^* = 1, \sqrt{3}, \sqrt{4}$, where q^* is the principal peak location (Figure S11B), characteristic of hexagonally packed cylinders (HEX). Upon heating to 125 °C, the PD3 sample exhibits an order-to−disorder transition (ODT) into a disordered polymer melt. Dynamic Mechanical Spectroscopy (DMS) measurements (Figure S12) establish T_{ODT} = 104 ± 5 °C for this specimen, consistent with SAXS experiments. Solvent cast blends of PD2 and PD3 exhibit DIS, HEX and BCC morphologies, as highlighted by SAXS patterns shown in Figure S13, where BCC order is associated with $q/q^* = 1, \sqrt{2}, \sqrt{3}$... Combined use of SAXS and DMS measurements (Figure S14) established the order-to-order transition (OOT) and ODT temperatures for 14 blend specimens with compositions $0 < \Phi_{PD2} < 1$, where Φ_{PD2} is the volume fraction of PD2. Based on the known interaction parameter,[29] $\chi_{PD} = (41.4/T) - 0.0237$, a $\chi\langle N\rangle$ versus f_{PEP} morphology diagram was constructed as shown in Figure 1, where $\langle N\rangle = \Phi_{PD2}N_{v,PD2} + (1 - \Phi_{PD2})N_{v,PD3}$ and N_v is the degree of polymerization (Table 1) referenced to the v =

https://doi.org/10.1021/acs.macromol.4c01146
Macromolecules 2024, 57, 7926−7940

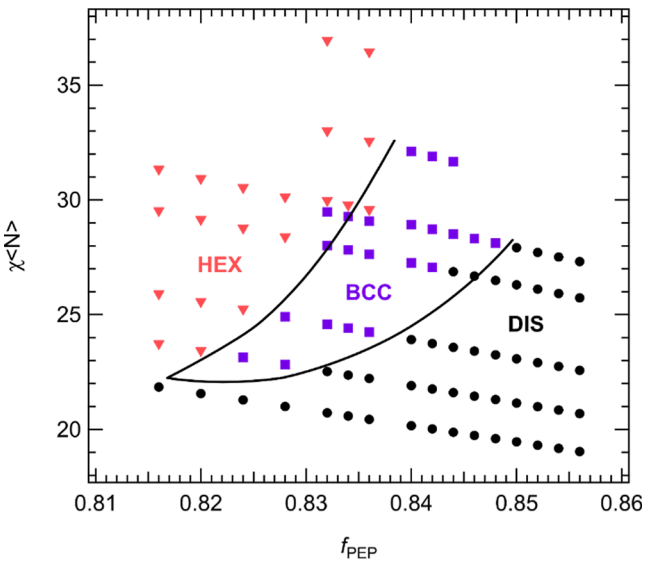

Figure 1. Morphology diagram $\chi\langle N\rangle$ versus f_{PEP} for PD2/PD3 blends based on SAXS analyses, revealing the formation of BCC (purple squares), HEX (red triangles), and DIS (black circles).

118 Å^3 segment volume. This illustration reveals a narrow BCC window that slants across the composition and temperature space, indicating that a single PD diblock copolymer with a suitable molecular weight and $f_D \approx 0.16$ would afford access to a BCC particle packing. Accordingly, sample PD1 was synthesized (Table 1) and SAXS patterns obtained between 25 and 140 °C (Figure 2A) confirm the anticipated phase behavior, HEX → BCC → DIS upon heating, while DMS measurements yield an order-to-order transition at T_{OOT} = 63 ± 3 °C and T_{ODT} = 112 ± 3 °C (Figure S15).

Design of PO Diblock Copolymers. Conformational asymmetry expands the sphere-forming window for PO diblock copolymers containing minority PEO blocks owing to b_O/b_P = 1.05. Based on our objective to probe particle radii (core and corona) that vary by up to ∼20% in PD/PO blends, we synthesized PO1 and PO2 diblocks with molecular weights bracketing PD1, guided by SCFT calculations. The design criteria included simultaneous access to T_{ODT} while forming a BCC phase over a wide range of temperatures, which dictated more asymmetric PO compositions than that characterizing PD1. Both polymers exhibit a BCC morphology in the ordered state, with T_{ODT} = 77 ± 5 °C and 175 ± 5 °C, for PO1 and PO2, respectively, as deduced from SAXS (Figure 2B,C) and DMS experiments (see Figures S16 and S17).

Heating PO1 to $T > T_{ODT}$ followed by cooling to 75 °C leads to rapid nucleation and growth of BCC order (<15 min), which upon cooling to 25 °C results in recovery of the same lattice constant (i.e., q^*) recorded for the solvent cast and 50 °C annealed material (Figure 2B). Disordering solvent cast PO2 by heating to 210 °C results in an ≈10% reduction in q^* relative to the ordered state value, which persists upon nucleation and growth of BCC order when cooled to 100 °C in <15 min. Apparently, disordering ($T > T_{ODT}$) facilitates formation of larger micelles upon subsequent cooling, implying that the solvent cast morphology was not at equilibrium. This result can be explained based on microphase separation at a finite polymer concentration during solvent evaporation, with subsequent particle shrinkage as the sample is dried further. This effect becomes increasingly severe with increasing molecular weight (i.e., increasing T_{ODT}), since microphase separation occurs at a higher solvent content leading to more exaggerated particle shrinkage,[30] consistent with the trends exhibited by PO1 and PO2. Additionally, the shift in q^* for PO2 at 25 °C is accompanied by "splitting" of the Bragg peaks, suggesting the presence of two micelle and unit cell sizes in the material—another nonequilibrium effect, potentially from the formation and growth of large grains of the new lattice size. Annealing solvent cast PO2 at 80 °C for 4 d after disordering at 160 °C eliminates the peak splitting accompanied by a 14% increase in the BCC lattice constant (Figure S18). Annealing for 24 h at 50 °C was performed for all samples since solvent casting and drying under vacuum alone did not induce ordering of PO2 into a BCC morphology. As shown in Figure S19, a PO2 sample that was solvent cast, dried and stored at room temperature for 4 d resulted in no Bragg reflections, whereas a sample solvent cast, dried, annealed at 50 °C for 24 h, and stored at room temperature for ∼7 d formed a well-ordered BCC structure with $q^* \approx 0.037$ Å^{-1}. A reversible q^*

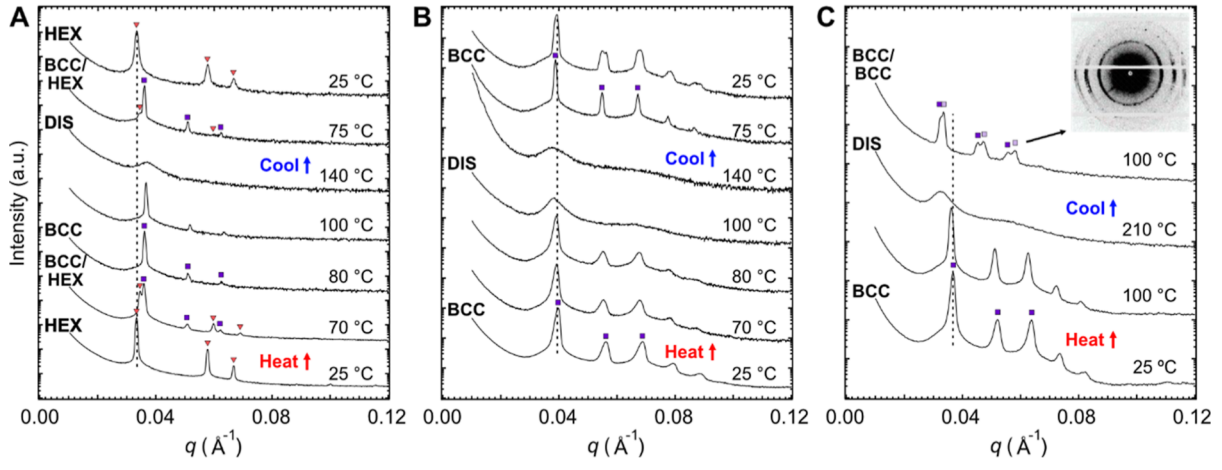

Figure 2. 1D SAXS intensity profiles for pure (A) PD1, (B) PO1, and (C) PO2 after solvent casting and annealing at 50 °C for 24 h. Purple squares and red triangles correspond to indexing for BCC and HEX, respectively. Dashed lines enable visual comparison of $q^*(T)$ referenced to 25 °C. The two distinct sets of purple squares in the top trace of panel C each index to BCC, suggesting the presence of two distinct micelle sizes. This is distinct from the behavior observed in panel B, where the peak splitting results from modest texture ("spottiness") in the 2D-SAXS pattern.

https://doi.org/10.1021/acs.macromol.4c01146
Macromolecules 2024, 57, 7926−7940

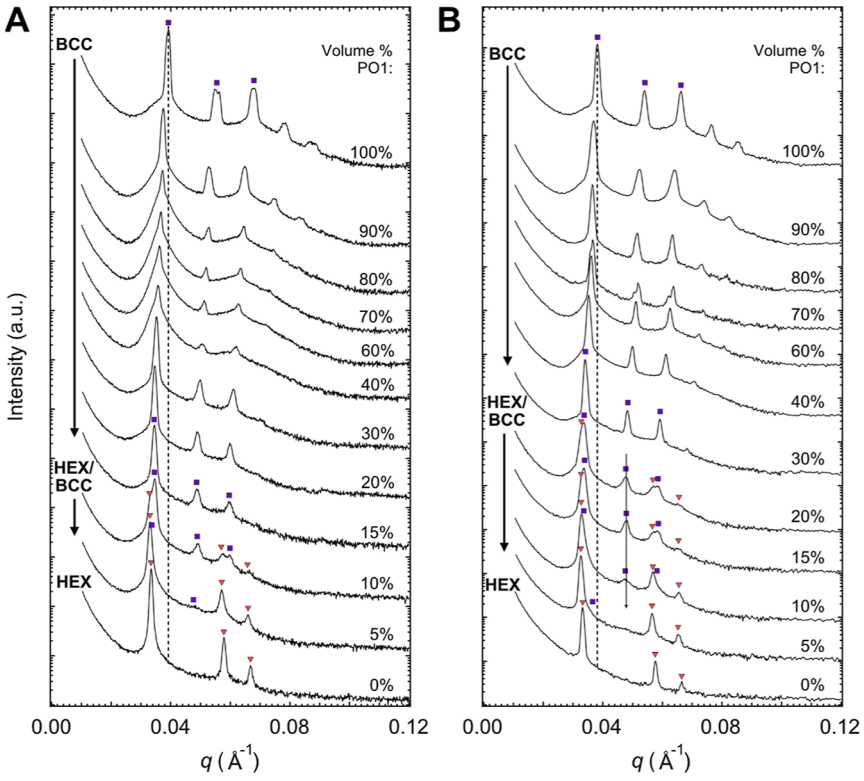

Figure 3. 1D SAXS traces for the PO1/PD1 blend obtained at 25 °C after annealing for (A) 10 min and (B) 48 h after cooling from a disordered state. Note that the Φ_{PO1} < 30% samples display peaks consistent with both HEX and BCC morphologies, whereas blends with Φ_{PO1} > 30% form only BCC.

obtained on heating and cooling indicates PO1 accesses equilibrium dimensions after 24 h of annealing at 50 °C.[31] Therefore, solvent casting and annealing at 50 °C for 24 h was utilized to obtain ordered phases in blends containing either PO1 or PO2 with PD1. However, we note that annealing at 50 °C for 24 h did not erase the metastable PO2 particle size created during solvent casting.

PEO is a semicrystalline polymer, which could complicate ordering of the PO block polymers due to breakout crystallization.[32] As shown in Figure S20B, DSC measurements reveal that PO1 and PO2 display PEO melting temperatures of T_m = 31 and 35 °C, respectively. However, deep undercooling is required to crystallize the PEO blocks, $T_c \cong -41$ °C and −36 °C for PO1 and PO2 respectively, when cooled at 10 °C/min (see Figure S20A), so that crystallization within the core domains of the microphase separated polymers does not occur for extended periods of time after cooling to room temperature from $T > T_m$. This was verified by WAXS, which showed no discernible diffraction peaks after storing samples at ambient temperature for ∼1 week.

BCC lattice parameters and average micelle radii R (including the particle core and corona) associated with the pure PO1, PO2, and PD1 BCC structures were calculated from the position of the principal scattering peaks. For a BCC packing, this corresponds to the (110) diffraction condition ($q^* = q_{110}$) with the lattice parameter given by $a = 2\pi\sqrt{2}/q_{110}$ and $4\pi R^3/3 = a^3/2$, based on 2 particles per unit cell. Note that each particle must assume a polyhedral (truncated cuboctahedron) shape in order to fill space without voids or density variations,[33] hence, the calculated micelle radii represent averages over all the associated polyhedron facets.

PO1/PD1 Blends. Blends containing Φ_{PO1} = 5, 10, 15, 20, 30, 40, 60, 70, 80, and 90% by volume PO1 in PD1 were solvent cast, heated to 140 °C ($>T_{ODT}$), cooled to and held at 70 °C and then ambient temperature (∼25 °C) each for 10 min, then measured by SAXS. As illustrated in Figure 3A, blends with Φ_{PO1} > 20% produced BCC order within this time frame, although the 40 to 80% mixtures are characterized by rather broad diffraction peaks indicative of relatively short-range order. Blends with 5 to 20% PO1 instead exhibit diffraction patterns that reflect a mixed HEX and BCC morphology. After 48 h at ambient temperature, this phase behavior persists, although the 40 to 80% blends evolve considerably sharper SAXS reflections with 4 or 5 orders of diffraction, consistent with a polycrystalline BCC structure. Phase separation (HEX/BCC) remains evident for the 5 to 20% PO1 mixtures. Additional SAXS measurements were conducted at various temperatures up to 140 °C; representative data are provided in Figure S21. A morphology diagram is presented in Figure 4, which shows a small window of HEX/BCC coexistence when $\Phi_{PO1} \leq 20\%$ and $T < 70$ °C, and BCC order throughout the remaining compositions and temperatures, with a narrow 2-phase BCC/DIS window separating order and disorder. We note that T_{ODT} is somewhat depressed at intermediate compositions relative to a linear combination of the pure component values. Overall, apart from the small 2-phase HEX/BCC window, the PO1/PD1 blends appear to produce solid solutions, where the two chemically distinct micelles are randomly distributed on a BCC lattice. This conclusion is supported by the systematic variation of ∼11% in q^* across the full range of compositions containing a BCC structure cooling from 140 °C and annealing at 25 °C for 48 h before measuring at 25 °C, as illustrated in Figure 5. This

https://doi.org/10.1021/acs.macromol.4c01146
Macromolecules 2024, 57, 7926−7940

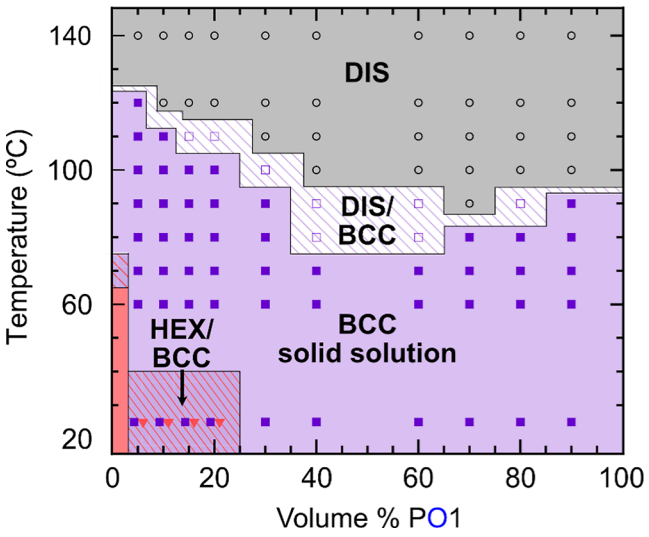

Figure 4. Morphology diagram for PO1/PD1 blends. All blends rapidly nucleate and grow a solid solution BCC phase on cooling from the disordered state within 15 min, and the phase behavior is reversible on heating and cooling.

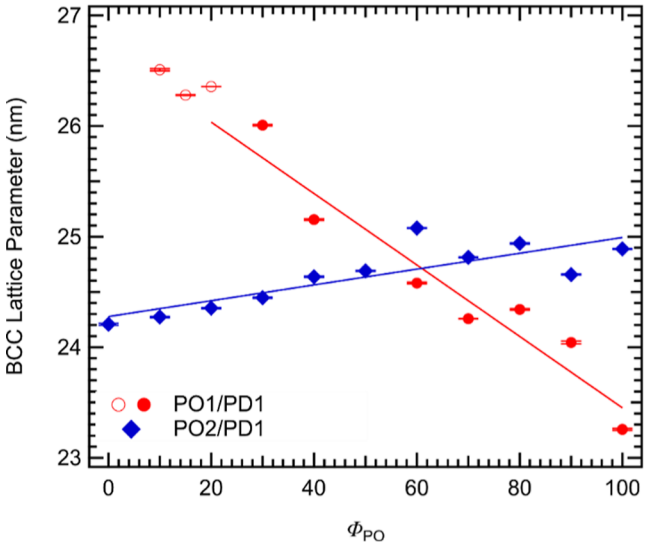

Figure 5. Plot of BCC lattice parameter versus Φ_{PO} for PO1/PD1 (red circles) and PO2/PD1 (blue diamonds). PO1/PD1 blends were processed by solvent casting and annealing at 50 °C for 24 h, then cooling from the disordered state (140 °C) and annealing at 25 °C for 48 h. PO2/PD1 blends were processed by solvent casting and annealing at 50 °C for 24 h, then subsequently heating for 10 min and measuring at 100 °C. Error bars reflect uncertainty in fitting the SAXS peaks associated with the (110), (200) and (211) reflections (see Figure S22). Points with $\Phi_{PO1} \leq 20\%$ were obtained from HEX/BCC coexisting states, where the (200) peak of the BCC structure was used to extract the domain spacing.

behavior satisfies Vegard's law (generally applied to metal alloys), which states that the lattice parameter in solid solutions scales linearly with the blend composition.[34] PD1 and PO1 display nearly identical q^* values at 140 °C (in the disordered state) implying nearly identical particle radii; assuming equivalence between the average DIS and BCC packing lengths,[33] $R_{PD1} \approx 11.8$ nm and $R_{PO1} \approx 11.6$ nm. These results indicate that the particle radii of PO1 and PD1 have different temperature dependences; we assign $\alpha = R_{PO1}/R_{PD1} \cong 0.9$ while noting this temperature dependence. The BCC lattice parameter after cooling and annealing is also compared to its initial value after solvent casting and annealing at 50 °C for 24 h in Figure S23, which shows minor deviations in domain spacing (<5%). This increase in lattice parameter upon disordering, cooling, and annealing reflects a small increase in micelle size.

PO2/PD1 Blends. Samples containing Φ_{PO2} = 10 to 90% PO2 mixed with PD1 in 10% increments were solvent cast at room temperature, annealed at 50 °C for 24 h, and examined at 25 °C by SAXS. The results, presented in Figure S24, index to BCC packings for $\Phi_{PO2} > 20\%$. Subsequently, each blend specimen was heated to and maintained at 100 °C for 10 min followed by acquisition of a SAXS pattern. As shown in Figure 6A, all these blends produced 3 to 5 diffraction peaks that we interpret as evidence of BCC solid solutions with nearly invariant lattice parameters as plotted in Figure 5. Additional heating leads to disorder or a mixed DIS/BCC state at 160 °C (Figure S25), as summarized by the morphology diagram in Figure 7A.

Next, the PO2/PD1 SAXS specimens were held at 160 °C for 20 min, cooled to, and held at 75 °C for 10 min, then cooled to 25 °C, and after 10 min, probed using SAXS, where the results are shown in Figure 6B. These mixtures behave differently than the PO1/PD1 blends when cooled from disorder to well below T_{ODT} (Figure 3A). Note that, except for the 80 and 90% blends, all these mixtures are disordered at 160 °C (see Figure S25). At intermediate compositions, $20\% \leq \Phi_{PO2} \leq 70\%$, nucleation and growth of order is suppressed, resulting in a state of liquid-like packing (LLP), or a combination of LLP and poorly formed BCC. Here we note that some of these blends are not homogeneous as evidenced by variations in the acquired SAXS patterns when the X-ray beam is moved across the 2 mm diameter sample holder (Figure S26).

Subsequently, these same PO2/PD1 blend specimens were held at ambient temperature for 20 h, heated to and annealed at 100 °C for 40 h, then cooled and examined again by SAXS at 25 °C (Figure 8). Remarkably, blends with $20\% \leq \Phi_{PO2} \leq 40\%$ and $\Phi_{PO2} = 70\%$ still failed to order as evidenced by a single broad scattering peak, evidencing very slow ordering kinetics in these blends. The $\Phi_{PO2} = 50\%$ specimen exhibits a new diffraction pattern that is distinctly different than that associated with BCC order, most notably evidenced by Bragg scattering at q values significantly smaller than q_{BCC}^*. We tentatively identify the associated morphology as a C14 Laves phase based on the indexing shown in Figure 9. Shifting the location in the X-ray beam of the cell holding the $\Phi_{PO2} = 50\%$ specimen that produced the nominal C14 phase led to variations in the SAXS pattern as shown in Figure S27, which is interpreted as position-dependent nucleation and growth of the ordered Laves phase. The presence of BCC Bragg reflections at two measurement locations (measurements 5 and 6 in Figure S27) lead us to assign this sample as BCC/C14 coexistence. The C14 structure is characterized by three distinct particle volumes, which occupy 127.0, 86.6, and 86.1% of the mean particle volume using the unconstrained diblock foam model.[35] Based on the SAXS data at 100 °C (Figure 9), R_{large} = 14.2 nm and R_{small} = 12.5 nm, corresponding to an average micelle size of 13.1 nm, which is slightly larger than the BCC structure with R = 12.8 nm at sample positions 5 and 6 (Figure S27). Based on the pure component micelle sizes R_{PO} = 14.3 nm and R_{PD} = 12.2 nm, we anticipate this C14

https://doi.org/10.1021/acs.macromol.4c01146
Macromolecules 2024, 57, 7926−7940

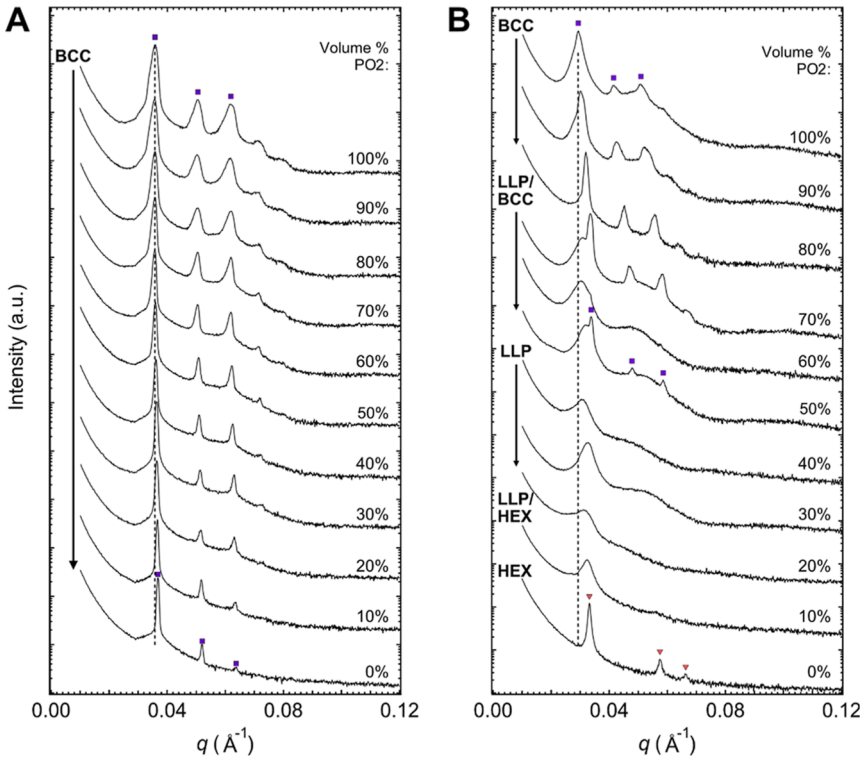

Figure 6. 1D SAXS traces of PO2/PD1 blends after (A) heating to 100 °C for 10 min and (B) cooling from 160 to 25 °C followed by a 10 min annealing time. Blends with 10 ≤ Φ_{PO2} ≤ 70% display a lack of long-range order on cooling, as evidenced by weak or no Bragg reflections.

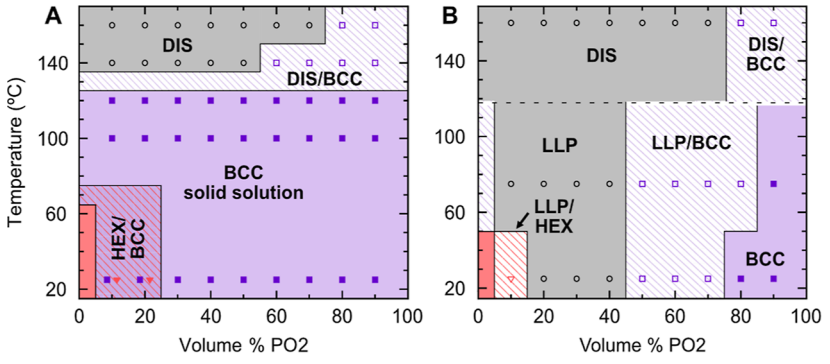

Figure 7. Morphology diagrams for PO2/PD1 blends on (A) heating from 25 to 160 °C from a solvent cast state and (B) annealed at 160 °C for 20 min and cooled; data obtained immediately after heating as reflected in panel A. Samples denoted LLP exhibit a single, broad SAXS feature below T_{ODT}.

morphology consists of larger PO micelles and smaller PD micelles.

To further characterize these blend morphologies, the high-q SAXS data for each BCC blend specimen annealed at 100 °C for 40 h was fit to a spherical form factor (Figure 8). As described in the Supporting Information (Figures S28−S30 and Table S1), the form factor scattering for the Φ_{PO} = 50% blend is fit equally well by a single particle radius (shown in Figure 9) or using the weighted sum of scattering intensities from PEO and PDMS spherical cores with dimensions and compositions consistent with a C14 Laves phase. Using the core radii (R_{core}) determined from the form factor fits and the total micelle radii (core and corona) deduced from q*, micelle core block volume fractions were calculated. If both diblocks had equivalent X-ray scattering contrast, or the PEO and PDMS blocks were fully mixed, the calculated micelle core block fraction would be equivalent to a weighted average of the minority block fractions f_O and f_D. However, the results shown in Figure 10 (and Table S1) demonstrate that the measured blend core volume fractions are similar to the core fraction of pure PO2 regardless of blend composition. Because the scattering contrast between PEP and PEO is ∼16× stronger than between PEP and PDMS, the blend form factor scattering is dominated by contributions from PO. As the fraction of PO decreases the intensity of the form factor scattering decreases, virtually disappearing for Φ_{PO2} ≤ 30%. Somewhat surprisingly, the calculated f_{core} for the C14 phase is much greater than that of pure PO. We attribute this to the stoichiometry of the observed structure, which should consist of 2/3 PD micelles, increasing the form factor scattering contribution from PD. Importantly, these results verify that the PEO and PDMS blocks do not mix.

Laves phase formation in the Φ_{PO2} = 50% mixture was reproduced by solvent casting a separate specimen, heating at

https://doi.org/10.1021/acs.macromol.4c01146
Macromolecules 2024, 57, 7926−7940

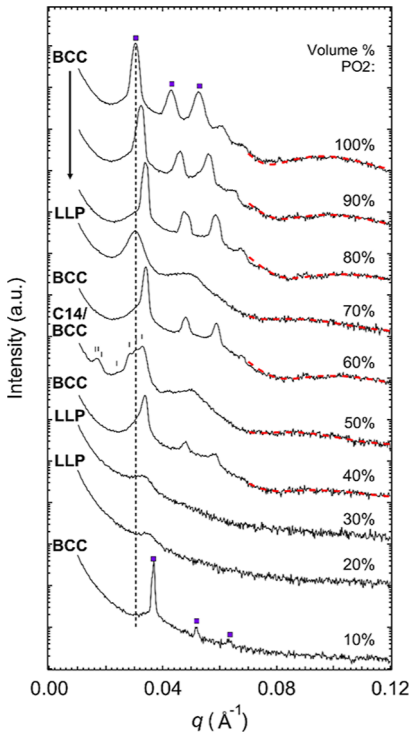

Figure 8. 1D SAXS data for PO2/PD1 blends after the following protocol: solvent cast and annealed at 50 °C for 24 h, heated to 160 °C for 20 min, cooled to 25 °C and held at this temperature for 20 h, then annealed at 100 °C for 40 h. Measurements are taken at 25 °C following the final annealing period. The red dashed curves show calculated spherical form factors (see Supporting Information for fitting details).

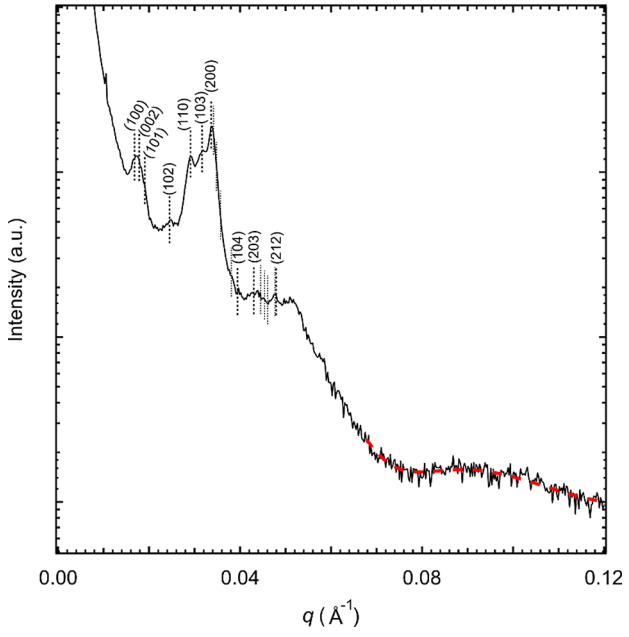

Figure 9. Indexing of a 50% PO2/PD1 sample at 100 °C, which was cooled from the disordered state and annealed for 20 h at 25 °C and 40 h at 100 °C, consistent with a C14 structure ($P6_3/mmc$) with lattice parameters a = 43.0 nm and c = 70.3 nm. The red dashed curve represents a spherical form factor calculation (see Supporting Information for fitting details).

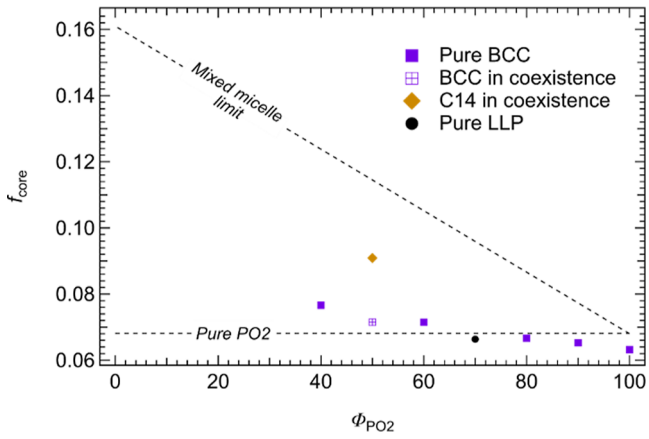

Figure 10. Values for f_{core} vs Φ_{PO2} calculated from q^* and form factor fits. See Supporting Information for full results and fitting details. Filled purple squares denote pure BCC phases, and the open purple square shows the BCC from BCC/C14 coexistence. The orange diamond gives the C14 value, and the black circle comes from the LLP trace. These data points are compared to the mixed micelle limit, calculated from an average of PO2 and PD1 volume fractions.

~1 °C/min to ~180 °C in a vacuum oven, cooling to 80 °C at ~1 °C/min, and annealing for 4 d at 80 °C. The corresponding SAXS traces (Figures S31 and S32) show weak C14 Bragg reflections superposed with well-defined BCC peaks (note that the low q features are not observable due to experimental apparatus limitations, nevertheless indexing for the (110), (103), (201), (202), and (203) reflections is shown). Other blend samples with Φ_{PO2} = 30, 40, 60, and 70% were prepared in a similar manner and display only BCC scattering after annealing at 100 °C for 4 days, as shown in Figure S31A. When heated to 120 °C, the Φ_{PO2} = 50% sample disorders, but does not nucleate a C14 structure after heating to 140 and 160 °C, followed by cooling to 75 and 25 °C and annealing for 24 h at 100 °C. To verify the hindered nucleation in PO2/PD1 blends, a second sample set was prepared with identical compositions as discussed above. The blends were heated and measured in 10−20 °C increments to 190 °C, followed by cooling to 100 and 25 °C, resulting in LLP structures between 20 and 80% PO2 as shown in Figure S33. Collectively, these results demonstrate that ordering is kinetically restricted in mixtures of PO2 and PD1.

The apparent nonequilibrium behavior displayed by the PO2/PD1 blends prompted us to explore longer thermal treatment protocols, focusing on the Φ_{PO2} = 34, 42, and 50% mixtures. Solvent cast specimens were heated at ~1 °C/min to 140 °C, held in the disordered state for about 10 min, followed by cooling at ~1 °C/min to 80 °C. Separate samples were held at 80 °C for 1, 4, or 8 d; these are referred to as 1-d, 4-d, and 8-d specimens. Following these thermal treatments, specimens were cooled to ambient temperature (~25 °C) and examined by SAXS. Subsequently heating and cooling these specimens produced the surprising results shown in Figures S34−S36 for Φ_{PO2} = 34 and 42%, and Figures 11, 12, and S37 for Φ_{PO2} = 50%. All three thermal treatments resulted in well-defined Bragg peaks that indicate BCC particle packing at 25 °C; the C14 phase observed previously for Φ_{PO2} = 50% (Figures 9 and S32) was notably absent. Heating the 1-d Φ_{PO2} = 50% specimen to 100 °C leads to disordering, and subsequent heating to 160 °C for 15 min followed by cooling to 100 °C resulted in an LLP state evidenced by broad diffraction

https://doi.org/10.1021/acs.macromol.4c01146
Macromolecules 2024, 57, 7926−7940

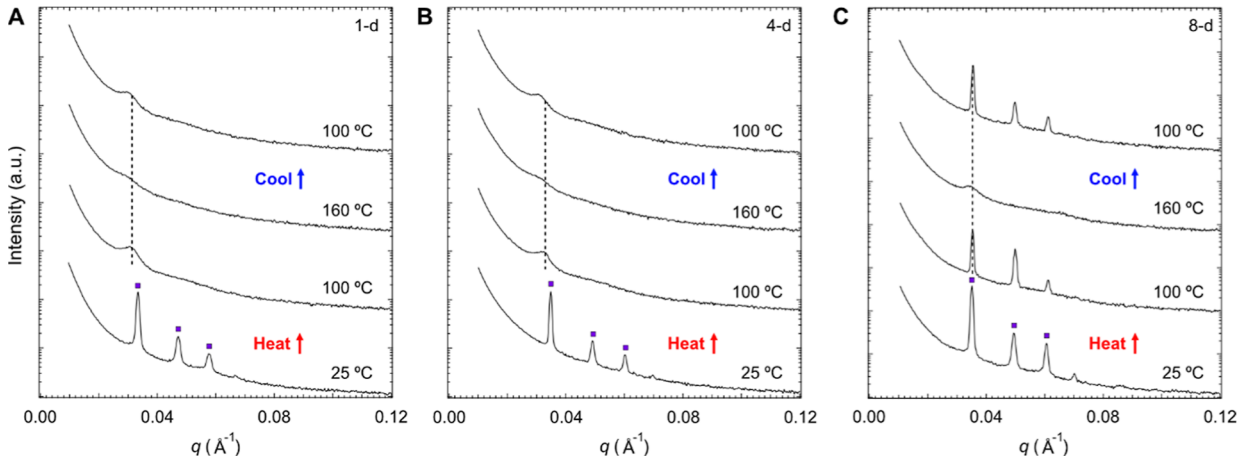

Figure 11. 1D SAXS traces of Φ_{PO2} = 50% blends which were disordered at 140 °C, cooled to 80 °C and held for either (A) 1 d, (B) 4 d, or (C) 8 d prior to measurement. The 1-d and 4-d blends do not nucleate a BCC structure on cooling from 160 °C, whereas the 8-d blend immediately renucleates a BCC phase with a nearly equivalent q^* to the disordered state.

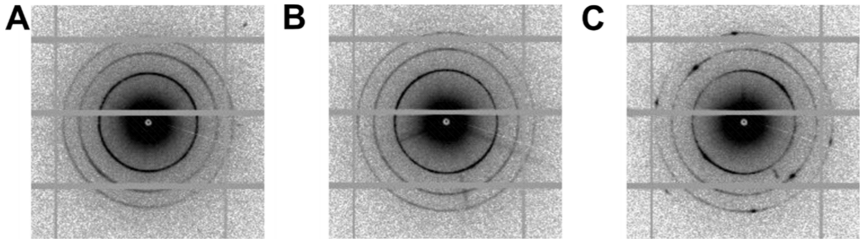

Figure 12. Representative 2D SAXS patterns for Φ_{PO2} = 50% blends annealed for (A) 1 d, (B) 4 d, and (C) 8 d. The development of spots in the 8-d sample is consistent with the growth of larger BCC grains. All three patterns are taken from the same sample location, and the other 8 sample locations are shown in Figure S37.

maxima. Similar results were obtained with the 4-d specimen. In contrast, the same thermal treatment applied to the 8-d specimen produced distinct BCC order at 100 °C. Qualitatively similar behavior was exhibited by the Φ_{PO2} = 34 and 42% blends (see Figure S34). These unusual results suggest that structural evolution occurs over a remarkably long time in the mixtures while in the BCC state at 80 °C. Additional evidence of such changes is found in the 2D SAXS patterns displayed in Figures 12 and S37 for Φ_{PO2} = 50%, along with Figures S35 and S36 for Φ_{PO2} = 34% and Φ_{PO2} = 42%. These illustrations reveal transformation from uniform scattering rings for the 1-d specimens, to distinctly spotty scattering patterns for the 8-d specimens. This indicates the evolution of relatively large BCC crystals after 8 d of annealing from an initially finely structured polycrystalline state after 1 d at 80 °C. All 8-d blend specimens rapidly grew well-ordered BCC states after heating to 210 °C ($T - T_{ODT} > 50$ °C) for 10 min followed by cooling to 100 °C (Figure S38). We return to these observations in the Discussion section.

Another indication of relatively slow structural changes that occur during annealing of the PO2/PD1 blends at 80 °C can be found in the precisely determined q^* values extracted from the SAXS patterns associated with the 1-d, 4-d, and 8-d specimens. Figure 13 depicts a plot of results obtained at 25, 100, and 160 °C for the Φ_{PO2} = 50% blend; data for Φ_{PO2} = 34% and Φ_{PO2} = 42% are shown in Figure S39, with information on fitting of the disordered state SAXS patterns presented in Figure S40. Clear reductions in the particle sizes occur between 1 and 8 d of isothermal annealing, reflected in

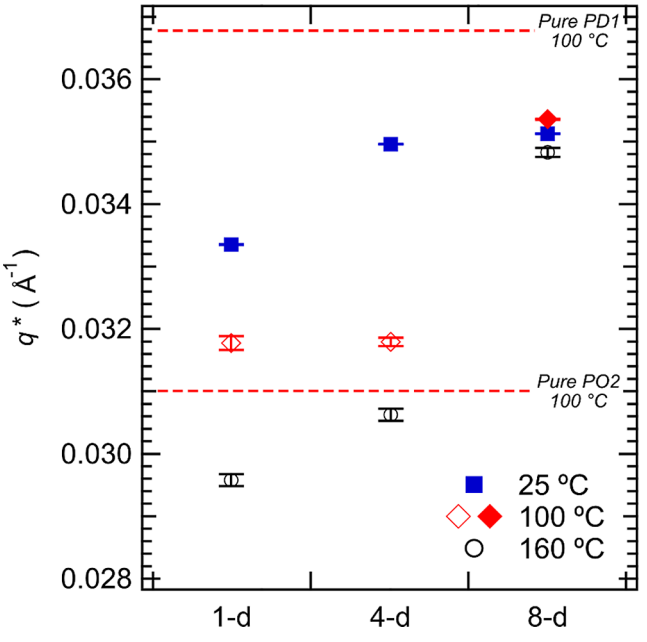

Figure 13. Temperature-dependent principal peak location, q^* (Å^{-1}), for 1-d, 4-d, and 8-d samples with Φ_{PO2} = 50%. Data points are shown on heating from 25 to 100 °C, and then to 160 °C at 10 °C/min with a 10 min annealing time at each temperature. Filled symbols are ordered and open symbols are disordered at each temperature. Dashed lines indicate q^* for both PD1 and PO2 for comparison. Fitting methods are described in Figure S40.

https://doi.org/10.1021/acs.macromol.4c01146
Macromolecules 2024, 57, 7926−7940

the q^* peak positions which are intermediate to the positions for pure PO2 and PD1.

DISCUSSION

The phase behavior of the asymmetric PO and PD diblock copolymers and blends described above illustrates the formation of equilibrium and nonequilibrium micellar morphologies derived from two chemically distinct components with tailored molecular weights and compositions. During conception of this project, we naively assumed the ratio of pure component micelle radii, R_{PO}/R_{PD}, would mimic the role of the relatively immutable atomic radii in binary metal alloys, which strongly influences phase behavior. The notable occurrence of myriad phases in metal alloys, and in particular tetrahedrally coordinated Frank−Kasper structures, is controlled in large part by the stoichiometric combination of elemental metals with specific ratios of atomic radii.[6,36] We have discovered that self-assembled space-filling block copolymer micelles are decidedly different, owing to mutable particle diameters that can change through fusion or fission, or chain exchange, degrees of freedom nonexistent with metal alloys.[37] Formation of Frank−Kasper phases in block copolymers, even (nominally) single component systems, has been shown to crucially rely on interparticle chain exchange, leading to the requisite ordered state symmetry-dependent distribution of particle volumes.[33] Moreover, the kinetics associated with such reconfigurations can result in long-lived nonequilibrium metastable states,[38] often controlled by large free-energy barriers that inhibit evolution of an equilibrium phase.[39] The present study exposes several such complexities, offering new insights regarding the feasibility of producing tailored phase behavior in binary diblock copolymer blends anticipated by recently published mean-field theory.[1,2]

PO1/PD1 Blends. Combining PO1 and PD1 results in the relatively rapid nucleation and growth of solid solutions with BCC packing below T_{ODT} across all compositions except for a narrow region around 25 °C and $\Phi_{PO1} \leq 20\%$, where HEX and BCC coexist (Figure 4). (Here we note that a simple cubic unit cell cannot be ruled out on the basis of the limited number of Bragg reflections (≤5) present in Figure 3A. However, formation of a CsCl structure requires stoichiometric balance, which is not satisfied across the range of compositions investigated.)[40] This behavior is readily rationalized based on the similar particle radii of the individual pure micelles: at 100 °C, SAXS analysis reveals $R_{PO1}/R_{PD1} \cong 0.96$. Here we note that these measurements represent an average over the truncated cuboctahedron shape associated with the packing of soft particles on a BCC lattice at uniform density, i.e., absent the formation of voids. In this nearly symmetric limit, the different particle cores play no role (other than enforcing particle formation and size) since the common PEP corona blocks shield contact between the thermodynamically incompatible PEO and PDMS core blocks as illustrated in Figure 14. Mixing the two types of micelles resembles solid solutions of binary metal alloys that satisfy the Hume-Rothery rules, i.e., $\Delta R/\langle R\rangle < 15\%$ for atomic radii R and common pure component crystal symmetries.[3]

PO2/PD1 Blends. Distinctly more complex phase behavior was exhibited by the PO2/PD1 blends, which can be attributed to a greater disparity in the pure component particle sizes: $R_{PO2}/R_{PD1} \cong 1.20$ following solvent casting, disordering, and annealing for 40 h at 100 °C. By coincidence, the solvent cast PO2/PD1 blends are characterized by nearly equal PD and PO particle sizes ($R_{PO2}/R_{PD1} \cong 1.03$ at 100 °C following solvent casting), which results in BCC solid solutions at 25 °C and when heated to 100 °C for 10 min (Figures 5 and 6A), analogous to the PO1/PD1 blends. Cooling from disorder (160 °C) generates BCC order after 10 min at 25 °C for the 0 and 80−100% PO2 mixtures, with LLP forming in the 10−70% PO2 blends. Annealing for 40 h at 100 °C (following cooling from 160 °C and annealing at 25 °C for 20 h) resulted in complex phase behavior over $20\% \leq \Phi_{PO2} \leq 70\%$; BCC packing is evident at 10, 80 and 90% PO2 (Figure 8).

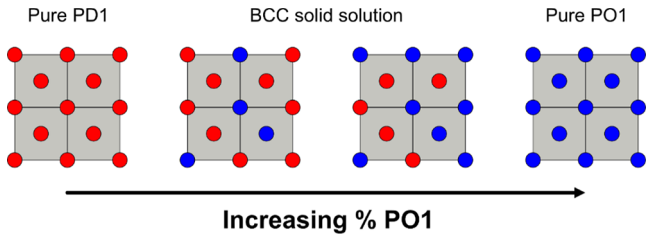

Figure 14. Illustration of BCC solid solution observed in PO1/PD1 blends along the [100]-direction. The blend fraction determines the average number of PO and PD micelles within a single unit cell.

At $\Phi_{PO2} = 50\%$, annealing at 100 °C for 40 h generated a C14 phase (Figure 9), although we hasten to reiterate that this structure appeared in only a portion of the SAXS specimen along with the BCC morphology; this was reproduced in a second specimen of $\Phi_{PO2} = 50\%$ (see Supporting Information Figures S31 and S32). Table S2 lists the extracted lattice parameters (c and a) and unit cell volume for 2 cases where the C14 phase was observed by SAXS at 25 °C; these lattice parameters are consistent within experimental uncertainty. Apparently, formation of the Laves phase is highly nucleation limited. Formation of tetrahedrally coordinated nuclei is presumably followed by rapid growth resulting in large grains of C14 revealed by moving the SAXS beam across the scattering specimen (Figure S27). Evidence of the Laves phase qualitatively agrees with the SCFT predictions by Magruder et al.[1] and Case et al.[2] that pure C14 compound formation is restricted to a very narrow band of intermediate compositions in AB/A′C diblock copolymer blends with different particle sizes. The theory anticipates maximum stability of Laves phases at a 14% difference in micelle radii, close to the experimentally obtained R_{PO2}/R_{PD1} after annealing. We note here that these calculations are based on conformationally symmetric diblock components, and a different set of χ parameters than those characterizing the PO/PD mixtures. Nevertheless, the predicted equilibrium phase diagrams provide guidance in interpreting the current experimental findings.

Insights regarding the nature of the LLP-to-BCC or LLP-to-C14/BCC transitions can be gleaned using the average particle sizes associated with each morphology. We associate the LLP scattering peak position with q^* of a BCC phase, as done previously.[41] As shown in Figure 6B, samples at $\Phi_{PO2} = 50$, 60, and 70% that display LLP/BCC coexistence exhibit a principal BCC peak (q^*) at higher q, or equivalently smaller average micelle size, than the LLP principal peak. We speculate that a change in average micelle size $\langle R\rangle$ is required to form BCC because $R_{PO2}/R_{PD1} \approx 1.20$, which interferes with formation of a BCC solid solution. Changing q^* for the BCC phase implies micellar fusion and/or fission events, since chain exchange alone cannot alter the particle density.[37] This observation is

https://doi.org/10.1021/acs.macromol.4c01146
Macromolecules 2024, 57, 7926−7940

also consistent with the data in Figures 6B and 8 which show samples exhibiting pure LLP with a smaller q^* than in the LLP/BCC or BCC states. In contrast, producing any Frank–Kasper phase including C14 requires different particle sizes along with specific micelle arrangements in the unit cells. Formation of C14 in a single diblock copolymer melt has been shown to occur with $\langle R_{LLP} \rangle \approx \langle R_{C14} \rangle$.[42,43] Deconvolution of the principal SAXS peaks for the 50%/50% PO2/PD1 blend that evolves through a BCC/LLP state (Figure S41) gives $\langle R_{LLP} \rangle$ = 13.6 nm and $\langle R_{BCC} \rangle$ = 12.9 nm compared to $\langle R_{C14} \rangle$ = 13.4 nm, all at 25 °C. This comparison is consistent with the notion that the supercooled LLP state can spawn a Laves phase only given a favorable combination of average PO and PD particle sizes.

Nucleation of the C14 phase in the PO2/PD1 blends is surprisingly dependent on the detailed thermal treatment of the mixtures. Solvent casting a Φ_{PO2} = 50% blend followed by heating to 160 °C, then annealing at 100 °C resulted in partial Laves phase formation (Figure 9). Yet heating 7 solvent cast Φ_{PO2} = 50% blend specimens to either 140, 160, 190, or 210 °C with subsequent annealing at ∼80 °C consistently produced BCC order. This inconsistency suggests that the free-energy that governs the phase behavior is nearly degenerate between BCC and C14, similar to what was reported based on SCFT for all the particle forming structures in single component diblock copolymer melts.[35,39]

Perspective. Due to the large corona blocks, individual micelle cores are virtually noninteracting. Therefore, the sole driving force to pack into a specific structure is the distribution of particle sizes that must fill space without forming voids, virtually a 3D puzzle of polyhedra, rendering it difficult to envision facile mechanisms of local particle dynamics. In hindsight, it is not surprising that spontaneously arranging the correct placement of 12 particles with 3 distinct particle radii into the specific positions necessary for C14 nucleation generally fails to compete with either BCC nucleation or LLP, as illustrated in Figure 15. This observation is in stark contrast with the extraordinary results reported by Cheng and co-workers, who discovered that mixtures of giant shape amphiphiles (GSAs) derived from polycyclic aromatic cores decorated with polyhedral oligomeric silsesquioxane (POSS) coronae self-assemble into a plethora of intermetallic structures, including FK σ, Laves C14 and C15, $NaZn_{13}$, $CaCu_5$, and AlB_2-type structures.[44−51] We note differences in aggregation number and particle stiffness as two possible explanations for the widespread stabilization of the superlattices reported by Cheng et al. that are decidedly absent in the diblock blend samples.

First, the aggregation number of each spherical motif has previously been used to rationalize stability of the Z phase in GSAs, another Frank–Kasper phase never reported in block polymers.[52,53] These GSAs self-assemble into mesoatoms of aggregation number N_{agg} ranging from 2 to 40. Hence, the degree of volume asymmetry associated with chain exchange (e.g., transitioning from two mesoatoms with N_{agg} = 10 to $N_{agg,1}$ = 9 and $N_{agg,2}$ = 11 imparts a 10% change in particle volume) is much more energetically costly than with the PO/PD blend system where $N_{agg} \approx 300$, wherein the volume asymmetry imparted by individual chain exchange events is <0.5%. Significantly, it will take numerous chain exchange events between diblock copolymer micelles to achieve the necessary distribution of particle volumes.

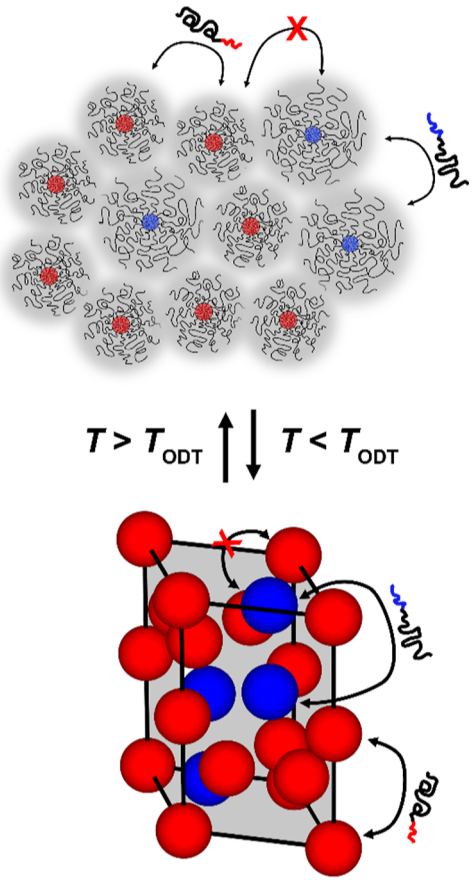

Figure 15. Packing of disordered micelles and particles into the Laves C14 phase in a diblock blend. Chain exchange is only present between individual cores comprising O or D, so that ordering into a C14 lattice is entirely driven by particle positions and volumes.

Second, the relative "softness" of the corona block in diblocks relative to GSAs favors the formation of BCC solid solution structures. The aromatic-based POSS outer shell found in many of the GSA blends is much stiffer than the shared majority PEP block in the PO/PD blends, which can support variable chain stretching required to form a BCC phase, even with some variation in particle volumes. Conversely, the POSS coronal region of GSA blends approaches the "hard-sphere" limit of metal alloys, where various low-symmetry phases form to accommodate the different particle volumes.

We designed the experiments summarized in Figures 11–13 (and S34–S40) to explore whether these subtle particle packing effects would manifest over long annealing times at modest undercooling below T_{ODT}. Blends with Φ_{PO2} = 34, 42, and 50% were subjected to a common thermal history (disordered at 140 °C, cooled to 80 °C and held for either 1, 4, or 8 d) then cooled to room temperature (nominally 25 °C). Each mixture was then heated to 100 °C followed by 160 °C then cooled back to 100 °C with SAXS patterns recorded at each step. This protocol was designed to explore whether particle restructuring occurred over time below or above T_{ODT}, and whether such changes were reflected in nucleation and growth of the BCC phase. The results are quite surprising. All three types of polymer blocks (PDMS, PEP, and PEO) are well above the glass transition temperatures ($T_g \leq -50$ °C) at all experimental conditions, and PEO block crystallization was deemed unlikely under ambient conditions, hence the

https://doi.org/10.1021/acs.macromol.4c01146
Macromolecules 2024, 57, 7926−7940

individual chain dynamics are fast at and above room temperature. Yet evidence of structural changes is found between 1 and 8 d of annealing at 80 °C, and after disordering, at all three compositions.

Following formation of BCC order from the disordered state, trends emerged both in the lattice and grain sizes during annealing. Upon increasing the annealing time from 1 to 8 d, the Φ_{PO2} = 42 and 50% samples display significant shifts in q^* at 25 and 100 °C (5 and 7%, respectively); this did not occur to the same extent in the Φ_{PO2} = 34% sample. Surprisingly, these trends are also evident after disordering at 160 °C, supporting the notion that the average particle size in the liquid state just above T_{ODT} can persist out of equilibrium for a considerable time.[54−57] These changes in q^* demonstrate that the average BCC particle size adjusts on time scales much longer than those associated with individual block or particle dynamics. As noted earlier, changing the average micelle diameter (i.e., number of particles per unit volume) requires fusion and/or fission events, since simple chain exchange leaves the particle density unchanged.[58]

Another striking feature in Figures 11 (and S34) is the marked change in T_{ODT} that accompanies annealing the BCC solid solutions formed by cooling from disorder. Each 8-d sample is characterized by a BCC structure that is stable up to nearly 160 °C, whereas the 1-d and 4-d samples disordered by 100 °C upon heating (except for the 42% 4-d specimen which ordered when heated to 100 °C). We believe the increase in T_{ODT} with increased annealing time also arises from a redistribution in particle sizes, evident in Figures 13 and S39. Micelle fusion and fission events are required to drive the shift in q^*, presumably refining the distribution of particle sizes toward a single average dimension across both PO and PD micelles. We believe this results in an increase in T_{ODT} due to a reduction in lattice strain associated with refining the broader mix of particle sizes generated upon cooling the solvent cast specimens from $T > T_{ODT}$. While none of the three blends (Φ_{PO2} = 34, 42 and 50%) nucleate and grow crystalline order within 15 min when cooled from 160 to 100 °C after 1 to 4 d of annealing at 80 °C, after 8 days at 80 °C all three rapidly (<15 min) develop BCC structure following the same thermal treatment. These experiments demonstrate that refinement of the particle size distribution in the PO2/PD1 blends is a remarkably slow process (ca. > 96 h), relative to the kinetics of ordering displayed by the PO1/PD1 blends, which require little particle resizing to nucleate and grow a BCC structure.[31,59−61] Moreover, heating to 160 °C (>T_{ODT}) for 10 min does not lead to particle size equilibration: the q^* observed in the disordered state depends on the thermal processing protocol, even when the ordered state q^* is similar. This observation is consistent with the conclusion drawn by Kim et al., who discovered that disordering a particle forming PI-PLA diblock copolymer then cooling to $T < T_{ODT}$ preserved either a BCC or C14 or C15 morphology established at low temperature, i.e. the disordered melt retained a "memory" of the ordered state.[39,58]

The concept of structural memory in the disordered state is also evident in the 8-d annealed samples, as the q^* in the disordered state mirrors that of the low temperature BCC phase. This does not occur in the 1-d and 4-d samples; these blends display a shift in q^* on disordering, which is maintained on cooling to T = 100 °C < T_{ODT}, where BCC order is not observed. This development of q^* is directly correlated with the average particle size in the disordered state and the degree of order in a sample upon cooling. We believe the shift to lower q^* on disordering is consistent with lattice strain and corresponding lower T_{ODT}'s for the 1-d and 4-d samples. Nucleating a strained BCC morphology likely leads to chains within the PO and PD micelles with more compressed and/or stretched configurations required to accommodate the mismatched particle sizes.

The tedious thermal protocols performed with the goal of stabilizing a low-symmetry phase further illustrate the nearly impossible task of predicting the nucleation tendencies of these diblock blends. Additionally, the macroscopic heterogeneity of the Laves-forming sample further complicates characterization of these mixtures. Concerted efforts were made to evaluate the morphologies of each sample at many locations within the DSC pan, however, instrument limitations hinder the ability to obtain a continuous "image" of the sample, unlike other techniques like transmission electron microscopy or atomic force microscopy.

CONCLUSIONS

Ordering of binary blends of particle forming PO and PD diblock copolymers is strongly dependent on the radii of the mutually immiscible micelles. Mixtures of nearly equal size particles, $\alpha = R_{PO}/R_{PD} \approx 0.9$, rapidly nucleate and grow BCC solid solutions upon cooling the melt to $T < T_{ODT}$. In contrast, $\alpha \approx 1.2$ results in complex ordering phenomena, including slow BCC ordering kinetics and sporadic formation of the C14 phase at blend compositions where SCFT predicts phase separation into BCC and Laves phases, surrounding a narrow range of compositions associated with a C14 phase field. This predominantly nonequilibrium behavior is attributed to two types of particle packing frustration: (1) inability to form a single particle size by chain exchange, necessitating slow and inefficient fusion and/or fission events in order to develop BCC order; and (2) barriers to positioning the different size micelles in order to accommodate Laves phase packing symmetry due to the space filling nature of the soft polyhedral shaped nanodomains.

These findings highlight dramatic differences between ordering in metal alloys and binary mixtures of diblock copolymer micelles. Equilibrium Laves phases readily nucleate and grow in mixtures of elemental metals driven largely by the fixed ratio of atomic radii, e.g. $MgZn_2$ (R_{Mg}/R_{Zn} = 1.20) and $MgCu_2$ (R_{Mg}/R_{Cu} = 1.25), which form C14 and C15 compounds, respectively.[3] Conversely, binary mixtures of nonexchangeable, soft, and jammed block copolymer micelles are inhibited from developing the required size distribution and configuration of dissimilar particles necessary to create the soft Laves phases, resulting in the slow evolution of BCC order. Ironically, nominally single component diblock copolymers can more easily accommodate both the positional and size distribution requirements for the formation of Frank−Kasper phases, including the Laves structures, by simple chain exchange.[33,39,42,43,58,62−71] Remarkably, simple one-component diblock copolymer melts mimic metal alloys in some ways, while two-component diblock copolymer blends do not.

ASSOCIATED CONTENT

Supporting Information

The Supporting Information is available free of charge at https://pubs.acs.org/doi/10.1021/acs.macromol.4c01146.

https://doi.org/10.1021/acs.macromol.4c01146
Macromolecules 2024, 57, 7926−7940

Experimental details and additional characterization data (PDF) (PDF)

AUTHOR INFORMATION

Corresponding Authors

Mahesh K. Mahanthappa − *Department of Chemical Engineering and Materials Science, University of Minnesota, Minneapolis, Minnesota 55455, United States;* orcid.org/0000-0002-9871-804X; Email: maheshkm@umn.edu

Frank S. Bates − *Department of Chemical Engineering and Materials Science, University of Minnesota, Minneapolis, Minnesota 55455, United States;* orcid.org/0000-0003-3977-1278; Email: bates001@umn.edu

Authors

Zachary M. Gdowski − *Department of Chemical Engineering and Materials Science, University of Minnesota, Minneapolis, Minnesota 55455, United States*

Samuel M. Swartzendruber − *Department of Chemical Engineering and Materials Science, University of Minnesota, Minneapolis, Minnesota 55455, United States*

Complete contact information is available at: https://pubs.acs.org/10.1021/acs.macromol.4c01146

Notes

The authors declare no competing financial interest.

ACKNOWLEDGMENTS

Financial support for this work was provided by the U.S. National Science Foundation under grant DMR-1801993. SAXS experiments were carried out at Sector 12 and Sector 5 of the Advanced Photon Source (APS). The Sector 5 DuPont-Northwestern-Dow Collaborative Access Team (DND-CAT) is supported by E.I. DuPont de Nemours & Co., the Dow Chemical Company, and Northwestern University. Use of the APS, an Office of Science User Facility operated for the U.S. Department of Energy (DOE) Office of Science by Argonne National Laboratory, was supported by the U.S. DOE under Contract no. DE-AC02-06CH11357. This research also used resources from Sector 11-BM CMS beamline of the National Synchrotron Light Source II, a U.S. Department of Energy (DOE) Office of Science User Facility operated for the DOE Office of Science by Brookhaven National Laboratory under Contract no. DE-SC0012704. Parts of this work, including lab source SAXS analyses, were carried out in the Characterization Facility at the University of Minnesota, which receives partial support from NSF through the UMN MRSEC (DMR-2011401). ^{1}H NMR spectra used in this study were collected on a Bruker Avance II HD 400 MHz spectrometer purchased by the Office of the Vice President of Research, the College of Science of and Engineering, and the Department of Chemistry at the University of Minnesota. We acknowledge Michael Hyatt for the purification of D_3, Parth Bhide for the purification of HMPA and TMSCl, and Joanna White and Camila Perales Rodriguez for SAXS measurements at APS Sector 5.

REFERENCES

(1) Magruder, B. R.; Park, S. J.; Collanton, R. P.; Bates, F. S.; Dorfman, K. D. Laves Phase Field in a Diblock Copolymer Alloy. *Macromolecules* **2022**, *55*, 2991−2998.

(2) Case, L. J.; Bates, F. S.; Dorfman, K. D. Tuning conformational asymmetry in particle-forming diblock copolymer alloys. *Soft Matter* **2023**, *19*, 90−97.

(3) Callister, W. D. *Materials Science and Engineering: An Introduction*; John Wiley: Hoboken, NJ, 2010.

(4) Frank, F. C.; Kasper, J. S. Complex Alloy Structures Regarded as Sphere Packings. I. Definitions and Basic Principles. *Acta Crystallogr.* **1958**, *11*, 184−190.

(5) Frank, F. C.; Kasper, J. S. Complex Alloy Structures Regarded as Sphere Packings. II. Analysis and Classification of Representative Structures. *Acta Crystallogr.* **1959**, *12*, 483−499.

(6) Sinha, A. K. Topologically Close-Packed Structures of Transition Metal Alloys. *Prog. Mater. Sci.* **1972**, *15*, 81−185.

(7) Friauf, J. B. The Crystal Structure of Magnesium Di-Zincide. *Phys. Rev.* **1927**, *29*, 34−40.

(8) Andersson, S. Structures Related to the β-tungsten or Cr_3Si Structure Type. *J. Solid State Chem.* **1978**, *23*, 191−204.

(9) Xie, N.; Liu, M.; Deng, H.; Li, W.; Qiu, F.; Shi, A. C. Macromolecular Metallurgy of Binary Mesocrystals via Designed Multiblock Terpolymers. *J. Am. Chem. Soc.* **2014**, *136*, 2974−2977.

(10) Frielinghaus, H.; Hermsdorf, N.; Sigel, R.; Almdal, K.; Mortensen, K.; Hamley, I. W.; Messé, L.; Corvazier, L.; Ryan, A. J.; Van Dusschoten, D.; Wilhelm, M.; Floudas, G.; Fytas, G. Blends of AB/BC Diblock Copolymers with a Large Interaction Parameter χ. *Macromolecules* **2001**, *34*, 4907−4916.

(11) Frielinghaus, H.; Hermsdorf, N.; Almdal, K.; Mortensen, K.; Messé, L.; Corvazier, L.; Fairclough, J. P. A.; Ryan, A. J.; Olmsted, P. D.; Hamley, I. W. Micro- vs. Macro-Phase Separation in Binary Blends of Poly(styrene)-Poly(isoprene) and Poly(isoprene)-Poly(ethylene oxide) Diblock Copolymers. *Europhys. Lett.* **2001**, *53*, 680−686.

(12) Ishizu, K.; Omote, A.; Fukutomi, T. Phase separation in binary block copolymer blends. *Polymer* **1990**, *31*, 2135−2140.

(13) Ketelaar, J. A. A. The Crystal Structure of Alloys of Zinc with the Alkali and Alkaline Earth Metals and of Cadmium with Potassium. *J. Chem. Phys.* **1937**, *5*, 668.

(14) Abbas, S.; Lodge, T. P. Superlattice Formation in a Binary Mixture of Block Copolymer Micelles. *Phys. Rev. Lett.* **2006**, *97*, 097803.

(15) Abbas, S.; Lodge, T. P. Superlattice Formation in Binary Mixtures of Block Copolymer Micelles. *Langmuir* **2008**, *24*, 6247−6253.

(16) Vigild, M. E. Mesomorphic Phase Behaviour of Low Molar Mass PEP-PDMS Diblock Copolymers Synthesized by Anionic Polymerization. Ph.D. Dissertation, University of Copenhagen, Roskilde, Denmark, 1997.

(17) Hillmyer, M. A.; Bates, F. S. Synthesis and Characterization of Model Polyalkane-Poly(ethylene oxide) Block Copolymers. *Macromolecules* **1996**, *29*, 6994−7002.

(18) Ness, J. S.; Brodil, J. C.; Bates, F. S.; Hahn, S. F.; Hucul, D. A.; Hillmyer, M. A. Molecular Weight Effects in the Hydrogenation of Model Polystyrenes Using Platinum Supported on Wide-Pore Silica. *Macromolecules* **2002**, *35*, 602−609.

(19) Lodge, T. P.; Hiemenz, P. C. *Polymer Chemistry*; Taylor & Francis Group: Boca Raton, FL, 2020.

(20) Schmidt, S. C.; Hillmyer, M. A. Morphological behavior of model poly(ethylene-alt-propylene)-b-polylactide diblock copolymers. *J. Polym. Sci., Part B: Polym. Phys.* **2002**, *40*, 2364−2376.

(21) Heiney, P. A. *Datasqueeze Software*; University of Pennsylvania, https://www.physics.upenn.edu/~heiney/datasqueeze. (accessed August 1, 2024).

(22) Lindsay, A. P.; Mueller, A. J.; Mahanthappa, M. K.; Lodge, T. P.; Bates, F. S. *1D SAXS Indexing Macro for Igor Pro*; Data Repository for the University of Minnesota, 2021.

(23) Matsen, M. W.; Bates, F. S. Conformationally asymmetric block copolymers. *J. Polym. Sci., Part B: Polym. Phys.* **1997**, *35*, 945−952.

(24) Misichronis, K.; Chen, J.; Imel, A.; Kumar, R.; Thostenson, J.; Hong, K.; Dadmun, M.; Sumpter, B. G.; Kennemur, J. G.; Hadjichristidis, N.; Mays, J. W.; Avgeropoulos, A. Investigations on

the Phase Diagram and Interaction Parameter of Poly(styrene-*b*-1,3-cyclohexadiene) Copolymers. *Macromolecules* **2017**, *50*, 2354−2363.
(25) Hamley, I. W.; O'Driscoll, B. M. D.; Lotze, G.; Moulton, C.; Allgaier, J.; Frielinghaus, H. Highly Asymmetric Phase Diagram of a Poly(1,2-octylene oxide)-Poly(ethylene oxide) Diblock Copolymer System Comprising a Brush-Like Poly(1,2-octylene oxide) Block. *Macromol. Rapid Commun.* **2009**, *30*, 2141−2146.
(26) Pochan, D. J.; Gido, S. P.; Zhou, J.; Mays, J. W.; Whitmore, M.; Ryan, A. J. Morphologies of microphase-separated conformationally asymmetric diblock copolymers. *J. Polym. Sci., Part B: Polym. Phys.* **1997**, *35*, 2629−2643.
(27) Floudas, G.; Vazaiou, B.; Schipper, F.; Ulrich, R.; Wiesner, U.; Iatrou, H.; Hadjichristidis, N. Poly(ethylene oxide-*b*-isoprene) Diblock Copolymer Phase Diagram. *Macromolecules* **2001**, *34*, 2947−2957.
(28) Fetters, L. J.; Lohse, D. J.; Richter, D.; Witten, T. A.; Zirkel, A. Connection Between Polymer Molecular Weight, Density, Chain Dimensions, and Melt Viscoelastic Properties. *Macromolecules* **1994**, *27*, 4639−4647.
(29) Almdal, K.; Hillmyer, M. A.; Bates, F. S. Influence of Conformational Asymmetry on Polymer-Polymer Interactions: An Entropic or Enthalpic Effect? *Macromolecules* **2002**, *35*, 7685−7691.
(30) Bates, F. S.; Berney, C. V.; Cohen, R. E. Microphase structure of solvent-cast diblock copolymers and copolymer-homopolymer blends containing spherical microdomains. *Macromolecules* **1983**, *16*, 1101−1108.
(31) Cavicchi, K. A.; Lodge, T. P. Domain Size Equilibration in Sphere-Forming Block Copolymers. *J. Polym. Sci., Part B: Polym. Phys.* **2003**, *41*, 715−724.
(32) Mueller, A. J.; Lindsay, A. P.; Jayaraman, A.; Lodge, T. P.; Mahanthappa, M. K.; Bates, F. S. Quasicrystals and Their Approximants in a Crystalline-Amorphous Diblock Copolymer. *Macromolecules* **2021**, *54*, 2647−2660.
(33) Lee, S.; Leighton, C.; Bates, F. S. Sphericity and Symmetry Breaking in the Formation of Frank-Kasper Phases from One Component Materials. *Proc. Natl. Acad. Sci. U.S.A.* **2014**, *111*, 17723−17731.
(34) Vegard, L. Die Konstitution der Mischkristalle und die Raumfüllung der Atome. *Z. Phys.* **1921**, *5*, 17−26.
(35) Reddy, A.; Buckley, M. B.; Arora, A.; Bates, F. S.; Dorfman, K. D.; Grason, G. M. Stable Frank-Kasper Phases of Self-Assembled, Soft Matter Spheres. *Proc. Natl. Acad. Sci. U.S.A.* **2018**, *115*, 10233−10238.
(36) Shoemaker, D. P.; Shoemaker, C. B. Concerning the Relative Numbers of Atomic Coordination Types in Tetrahedrally Close Packed Metal Structures. *Acta Crystallogr., Sect. B* **1986**, *42*, 3−11.
(37) Lodge, T. P.; Seitzinger, C. L.; Seeger, S. C.; Yang, S.; Gupta, S.; Dorfman, K. D. Dynamics and Equilibration Mechanisms in Block Copolymer Particles. *ACS Polym. Au* **2022**, *2*, 397−416.
(38) Gillard, T. M.; Lee, S.; Bates, F. S. Dodecagonal Quasicrystalline Order in a Diblock Copolymer Melt. *Proc. Natl. Acad. Sci. U.S.A.* **2016**, *113*, 5167−5172.
(39) Kim, K.; Schulze, M. W.; Arora, A.; Lewis, R. M.; Hillmyer, M. A.; Dorfman, K. D.; Bates, F. S. Thermal Processing of Diblock Copolymer Melts Mimics Metallurgy. *Science* **2017**, *356*, 520−523.
(40) Graef, M. D.; McHenry, M. E. *Structure of Materials: An Introduction to Crystallography, Diffraction and Symmetry*; Cambridge University Press, 2012.
(41) Lindsay, A. P.; Cheong, G. K.; Peterson, A. J.; Weigand, S.; Dorfman, K. D.; Lodge, T. P.; Bates, F. S. Complex Phase Behavior in Particle-Forming AB/AB′ Diblock Copolymer Blends with Variable Core Block Lengths. *Macromolecules* **2021**, *54*, 7088−7101.
(42) Nouri, B.; Chen, C. Y.; Huang, Y. S.; Mansel, B. W.; Chen, H. L. Emergence of a Metastable Laves C14 Phase of Block Copolymer Micelle Bearing a Glassy Core. *Macromolecules* **2021**, *54*, 9195−9203.
(43) Nouri, B.; Chen, C.-Y.; Lin, J.-M.; Chen, H.-L. Phase Control of Colloid-like Block Copolymer Micelles by Tuning Size Distribution via Thermal Processing. *Macromolecules* **2022**, *55*, 9820−9832.
(44) Lei, H.; Li, X.-H.; Liu, Y.; Liu, X.-Y.; Li, W.-Y.; Yan, X.-Y.; Huang, M.; Cheng, S. Z. D.; Huang, J. Diverse superlattices constructed via perylene bisimide type of giant shape amphiphiles: Assisted with unimolecular nanoparticles. *Thermochim. Acta* **2023**, *719*, 179411.
(45) Lei, H.; Liu, Y.; Liu, T.; Guo, Q. Y.; Yan, X. Y.; Wang, Y.; Zhang, W.; Su, Z.; Huang, J.; Xu, W.; Bian, F. G.; Huang, M.; Cheng, S. Z. D. Unimolecular Nanoparticles toward More Precise Regulations of Self-Assembled Superlattices in Soft Matter. *Angew. Chem., Int. Ed.* **2022**, *61*, No. e202203433.
(46) Wang, Y.; Huang, J.; Yan, X. Y.; Lei, H.; Liu, X. Y.; Guo, Q. Y.; Liu, Y.; Liu, T.; Huang, M.; Bian, F.; Su, Z.; Cheng, S. Z. D. Soft Alloys Constructed with Distinct Mesoatoms via Self-Sorting Assembly of Giant Shape Amphiphiles. *Angew. Chem., Int. Ed.* **2022**, *61*, No. e202200637.
(47) Liu, Y.; Liu, T.; Yan, X.-Y.; Guo, Q.-Y.; Lei, H.; Huang, Z.; Zhang, R.; Wang, Y.; Wang, J.; Liu, F.; Bian, F.-G.; Meijer, E. W.; Aida, T.; Huang, M.; Cheng, S. Z. D. Expanding quasiperiodicity in soft matter: Supramolecular decagonal quasicrystals by binary giant molecule blends. *Proc. Natl. Acad. Sci. U.S.A.* **2022**, *119*, No. e2115304119.
(48) Yan, X.-Y.; Guo, Q.-Y.; Liu, X.-Y.; Wang, Y.; Wang, J.; Su, Z.; Huang, J.; Bian, F.; Lin, H.; Huang, M.; Lin, Z.; Liu, T.; Liu, Y.; Cheng, S. Z. D. Superlattice Engineering with Chemically Precise Molecular Building Blocks. *J. Am. Chem. Soc.* **2021**, *143*, 21613−21621.
(49) Liu, Y.; Liu, T.; Yan, X. Y.; Guo, Q. Y.; Wang, J.; Zhang, R.; Zhang, S.; Su, Z.; Huang, J.; Liu, G. X.; Zhang, W.; Zhang, W.; Aida, T.; Yue, K.; Huang, M.; Cheng, S. Z. D. Mesoatom Alloys Via Self-Sorting Approach of Giant Molecules Blends. *Giant* **2020**, *4*, 100031.
(50) Li, X.-H.; Kuang, X.; Liu, X.-Y.; Lei, H.; Yan, X.-Y.; Li, W.; Deng, Y.; Wu, Y.; Guo, Q.-Y.; Cheng, S. Z. D. Exploring fullerene-based superlattices self-assembled via giant molecules. *Giant* **2023**, *16*, 100196.
(51) Liu, X.-Y.; Yan, X.-Y.; Liu, Y.; Qu, H.; Wang, Y.; Wang, J.; Guo, Q.-Y.; Lei, H.; Li, X.-H.; Bian, F.; Cao, X.-Y.; Zhang, R.; Wang, Y.; Huang, M.; Lin, Z.; Meijer, E. W.; Aida, T.; Kong, X.; Cheng, S. Z. D. Self-assembled soft alloy with Frank-Kasper phases beyond metals. *Nat. Mater.* **2024**, *23*, 570−576.
(52) Su, Z.; Hsu, C. H.; Gong, Z.; Feng, X.; Huang, J.; Zhang, R.; Wang, Y.; Mao, J.; Wesdemiotis, C.; Li, T.; Seifert, S.; Zhang, W.; Aida, T.; Huang, M.; Cheng, S. Z. D. Identification of a Frank-Kasper *Z* phase from Shape Amphiphile Self-Assembly. *Nat. Chem.* **2019**, *11*, 899−905.
(53) Huang, J.; Zhang, R.; Wang, Y.; Su, Z.; Yan, X. Y.; Guo, Q. Y.; Liu, T.; Liu, Y.; Lei, H.; Huang, M.; Zhang, W.; Cheng, S. Z. D. Rational Route Toward the Frank-Kasper *Z* Phase: Effect of Precise Geometrical Tuning on the Supramolecular Assembly of Giant Shape Amphiphiles. *Macromolecules* **2021**, *54*, 7777−7785.
(54) Dormidontova, E. E.; Lodge, T. P. The Order-Disorder Transition and the Disordered Micelle Regime in Sphere-Forming Block Copolymer Melts. *Macromolecules* **2001**, *34*, 9143−9155.
(55) Wang, X.; Dormidontova, E. E.; Lodge, T. P. The Order-Disorder Transition and the Disordered Micelle Regime for Poly(ethylenepropylene-*b*-dimethylsiloxane) Spheres. *Macromolecules* **2002**, *35*, 9687−9697.
(56) Cheong, G. K.; Dorfman, K. D. Disordered Micelle Regime in a Conformationally Asymmetric Diblock Copolymer Melt. *Macromolecules* **2021**, *54*, 9868−9878.
(57) Wang, J.; Wang, Z.-G.; Yang, Y. Nature of Disordered Micelles in Sphere-Forming Block Copolymer Melts. *Macromolecules* **2005**, *38*, 1979−1988.
(58) Kim, K.; Arora, A.; Lewis, R. M.; Liu, M.; Li, W.; Shi, A. C.; Dorfman, K. D.; Bates, F. S. Origins of Low-Symmetry Phases in Asymmetric Diblock Copolymer Melts. *Proc. Natl. Acad. Sci. U.S.A.* **2018**, *115*, 847−854.
(59) Cavicchi, K. A.; Lodge, T. P. Self-Diffusion and Tracer Diffusion in Sphere-Forming Block Copolymers. *Macromolecules* **2003**, *36*, 7158−7164.
(60) Papadakis, C. M.; Rittig, F.; Almdal, K.; Mortensen, K.; Štěpánek, P. Collective dynamics and self-diffusion in a diblock

https://doi.org/10.1021/acs.macromol.4c01146
Macromolecules 2024, 57, 7926−7940

copolymer melt in the body-centered cubic phase. *Eur. Phys. J. E* **2004**, *15*, 359−370.
(61) Rittig, F.; Kärger, J.; Papadakis, C. M.; Fleischer, G.; Štěpánek, P.; Almdal, K. Self-diffusion investigations on a series of PEP-PDMS diblock copolymers with different morphologies by pulsed field gradient NMR. *Phys. Chem. Chem. Phys.* **1999**, *1*, 3923−3931.
(62) Lee, S.; Bluemle, M. J.; Bates, F. S. Discovery of a Frank-Kasper σ Phase in Sphere-Forming Block Copolymer Melts. *Science* **2010**, *330*, 349−353.
(63) Uddin, M. H.; Rodriguez, C.; López-Quintela, A.; Leisner, D.; Solans, C.; Esquena, J.; Kunieda, H. Phase Behavior and Microstructure of Poly(oxyethylene)-Poly(dimethylsiloxane) Copolymer Melt. *Macromolecules* **2003**, *36*, 1261−1271.
(64) Bates, M. W.; Lequieu, J.; Barbon, S. M.; Lewis, R. M.; Delaney, K. T.; Anastasaki, A.; Hawker, C. J.; Fredrickson, G. H.; Bates, C. M. Stability of the A15 phase in Diblock Copolymer Melts. *Proc. Natl. Acad. Sci. U.S.A.* **2019**, *116*, 13194−13199.
(65) Schulze, M. W.; Lewis, R. M.; Lettow, J. H.; Hickey, R. J.; Gillard, T. M.; Hillmyer, M. A.; Bates, F. S. Conformational Asymmetry and Quasicrystal Approximants in Linear Diblock Copolymers. *Phys. Rev. Lett.* **2017**, *118*, 207801.
(66) Jeon, S.; Jun, T.; Jo, S.; Ahn, H.; Lee, S.; Lee, B.; Ryu, D. Y. Frank-Kasper Phases Identified in PDMS-*b*-PTFEA Copolymers with High Conformational Asymmetry. *Macromol. Rapid Commun.* **2019**, *40*, 1900259.
(67) Jeon, S.; Jun, T.; Jeon, H. I.; Ahn, H.; Lee, S.; Lee, B.; Ryu, D. Y. Various Low-Symmetry Phases in High-χ and Conformationally Asymmetric PDMS-*b*-PTFEA Copolymers. *Macromolecules* **2021**, *54*, 9351−9360.
(68) Jeon, S.; Jun, T.; Jo, S.; Kim, K.; Lee, B.; Lee, S.; Ryu, D. Y. Modifying Frank-Kasper Mesophases by Modulating Chain Configuration in PDMS-*b*-PTFEA Copolymers. *Macromolecules* **2022**, *55*, 8049−8057.
(69) Papadakis, C. M.; Almdal, K.; Mortensen, K.; Vigild, M. E.; Štěpánek, P. Unexpected Phase Behavior of an Asymmetric Diblock Copolymer. *J. Chem. Phys.* **1999**, *111*, 4319−4326.
(70) Lindsay, A. P.; Jayaraman, A.; Peterson, A. J.; Mueller, A. J.; Weigand, S.; Almdal, K.; Mahanthappa, M. K.; Lodge, T. P.; Bates, F. S. Reevaluation of Poly(ethylene-*alt*-propylene)-*block*-Polydimethylsiloxane Phase Behavior Uncovers Topological Close-Packing and Epitaxial Quasicrystal Growth. *ACS Nano* **2021**, *15*, 9453−9468.
(71) Dorfman, K. D. Frank-Kasper Phases in Block Polymers. *Macromolecules* **2021**, *54*, 10251−10270.

https://doi.org/10.1021/acs.macromol.4c01146
Macromolecules 2024, 57, 7926−7940